

# Author Queries

*Journal:* Interface Focus

*Manuscript:* rsfs20190123

As the publishing schedule is strict, please note that this might be the only stage at which you are able to thoroughly review your paper.

Please pay special attention to author names, affiliations and contact details, and figures, tables and their captions.

The corresponding author must provide an ORCID ID if they haven't done so already. If you or your co-authors have an ORCID ID please supply this with your corrections. More information about ORCID can be found at <http://orcid.org/>.

No changes can be made after publication.

- Q1** Please check the edit made to article title.
- Q2** Please supply the year of publication in the reference [32].

**Cite this article:** Luraghi G *et al.* 2020Q1 Applicability assessment of a stent-retriever thrombectomy finite element model. *Interface Focus* 20190123.  
<http://dx.doi.org/10.1098/rsfs.2019.0123>

Accepted: 23 September 2020

One contribution of 10 to a theme issue 'Computational biomedicine. Part II, organs and systems'.

**Subject Areas:**

biomedical engineering, biomechanics

**Keywords:**

INSIST, thrombectomy, acute ischaemic stroke (AIS), stent-retriever, finite-element analysis (FEA)

**Author for correspondence:**

Giulia Luraghi

e-mail: [giulia.luraghi@polimi.it](mailto:giulia.luraghi@polimi.it)

\*The INSIST investigators are given in the Appendix.

## Applicability assessment of a stent-retriever thrombectomy finite element model

Q1

Giulia Luraghi<sup>1</sup>, Jose Felix Rodriguez Matas<sup>1</sup>, Gabriele Dubini<sup>1</sup>, Francesca Berti<sup>1</sup>, Sara Bridio<sup>1</sup>, Sharon Duffy<sup>2</sup>, Anushree Dwivedi<sup>2</sup>, Ray McCarthy<sup>2</sup>, Behrooz Fereidoonzhad<sup>3</sup>, Patrick McGarry<sup>3</sup>, Charles B. L. M. Majoie<sup>4</sup>, Francesco Migliavacca<sup>1</sup> and on behalf of the INSIST investigators\*<sup>1</sup>Department of Chemistry, Materials and Chemical Engineering, Politecnico di Milano, Milan, Italy<sup>2</sup>Cerenovus, Neuro Technology Center, Galway, Ireland<sup>3</sup>Department of Biomedical Engineering, National University of Ireland Galway, Galway, Ireland<sup>4</sup>Departments of Radiology and Nuclear Medicine, Academic Medical Center, Amsterdam, The Netherlands

ID GL, 0000-0002-0434-8544

An acute ischaemic stroke (AIS) appears when a blood clot blocks the blood flow in a cerebral artery. Intra-arterial thrombectomy, a mini-invasive procedure based on stent technology, is a mechanical available treatment to extract the clot and restore the blood circulation. After stent deployment, the clot, trapped in the stent struts, is pulled along with the stent towards a receiving catheter. Recent clinical trials have confirmed the effectiveness and safety of mechanical thrombectomy. However, the procedure requires further investigation. The aim of this study is the development of a numerical finite-element-based model of the thrombectomy procedure. *In vitro* thrombectomy tests are performed in different vessel geometries and one simulation for each test is carried out to verify the accuracy and reliability of the proposed numerical model. The results of the simulations confirm the efficacy of the model to replicate all the experimental setups. Clot's stress and strain fields from the numerical analysis, which vary depending on the geometric features of the vessel, could be used to evaluate the possible fragmentation of the clot during the procedure. The proposed *in vitro*/*in silico* comparison aims at assessing the applicability of the numerical model and at providing validation evidence for the specific *in vivo* thrombectomy outcomes prediction.

**1. Introduction**

An acute ischaemic stroke (AIS) occurs when an artery that supplies blood to the brain is blocked by a blood clot (thrombus), which is a solidified mass of blood cells, platelets, fibrin and other blood components occurring as a result of blood coagulation. Rarely, occlusive clots may also consist of non-thrombus components such as fat emboli, tumour tissue, calcifications and the like. In the majority of AIS cases, the clot is formed elsewhere and embolized to the vessel it eventually occludes, although *in situ* occlusive thrombi also occur. Red thrombi, red blood cell (RBC) dominant, are understood to form where the blood flow is slow and the fibrin network entraps the RBCs, while white thrombi, fibrin dominant, are generated under high shear flow and inflammatory conditions [1]. Mechanical properties of blood clot strongly depend on the clot composition [1]. Common origins of embolic thrombi are the heart, atherosclerotic plaques, or from vessel wall dissections.

Detection of the location of the intracranial occlusion must be done in a fast and accurate way to ensure an appropriate selection of treatment and its speedy

64 delivery [2]. Treatment of AIS is aimed at restoring blood  
65 flow in the affected cerebral arteries as quickly as possible.  
66 *Time is crucial in stroke*—2 million neurons are lost every  
67 second without reperfusion [3]. The main diagnostic imaging  
68 techniques used to identify the clot location are computed  
69 tomography (CT) and magnetic resonance imaging (MRI).

70 There are currently two main therapies to treat an ischaemic  
71 stroke: (i) medical therapy using thrombolytic agents (thrombo-  
72 lysis) and (ii) interventional therapy to remove the clot using  
73 mechanical thrombectomy. The latter being indicated for  
74 large vessel occlusions of the neurovasculature. Thrombolysis  
75 became available recently and involves the administration of  
76 tissue plasminogen activator 3–4.5 h after the onset of a  
77 stroke. Most recently, intra-arterial mechanical thrombectomy  
78 has emerged as a widespread clinical intervention technique  
79 in the treatment of stroke [4]. Currently, a combined approach  
80 of thrombolysis and mechanical thrombectomy is recommen-  
81 ded for the treatment of AIS involving large vessel occlusion.  
82 Mechanical thrombectomy interventions are carried out with  
83 the aid of angiography to ensure the correct positioning of the  
84 devices relative to the occluded vessel.

85 Thrombectomy device design has two classifications  
86 based on their mode of action: (i) aspiration catheters and  
87 (ii) stent-retrievers. Aspiration catheters may be used without  
88 stent-retrievers; however, stent-retriever use usually includes  
89 some element of aspiration, either through a guide catheter  
90 placed in the extracranial internal carotid artery (ICA) or  
91 using a distal access catheter which can be placed close to  
92 the occlusion in smaller intracranial vessels. The superiority  
93 of one approach over the other is an ongoing subject of  
94 debate among neurointerventionalists [5–7]. Effectiveness of  
95 the thrombectomy approach taken is measured in terms  
96 of speed of revascularization, reperfusion grade, patient  
97 outcome, ease-of-use and cost of the procedure. The revascu-  
98 larization of the affected vessels is strongly associated with  
99 improved clinical outcomes for patients [8].

100 Stent-retrievers rely on the mechanical removal of the  
101 thrombus by means of a nickel-titanium (NiTi) self-expandable  
102 stent at the end of a flexible wire, delivered in a crimped  
103 configuration in a microcatheter and positioned across the  
104 thrombus. Once in position, the stent-retriever is deployed  
105 by withdrawing the microcatheter (even at this stage, the  
106 expanded stent may restore the blood flow by compressing  
107 the clot between the stent-retriever and the arterial wall).  
108 After deploying the stent-retriever, the clot, trapped in the  
109 stent struts, is pulled along with the stent towards a receiving  
110 catheter. In many cases, this operation is performed under  
111 arrested flow conditions achieved by a balloon inflated in a  
112 guide catheter positioned at the ICA at the skull base.  
113 A number of stents-retriever device designs are currently  
114 being used in clinical practices [9], and a number of clinical  
115 trials are currently ongoing [8,10–12]. In this regard, the seminal  
116 MR CLEAN clinical trial [13], a multicentre randomized clinical  
117 trial of endovascular treatment (EVT) for AIS in the Nether-  
118 lands, confirmed the effectiveness and safety of stent-retriever  
119 thrombectomy devices and demonstrated their improved out-  
120 come when combined with best medical therapy compared to  
121 thrombolysis alone.

122 However, despite its increasing clinical application,  
123 thrombectomy may result in some adverse outcomes, such as  
124 thrombus embolization to distal vessels caused by disruption  
125 of the clot during crossing, deployment or retrieval [14], embo-  
126 lization of clot to new vascular territories, hemorrhagic events

and vessel wall damage [15,16]. Procedural success also greatly  
depends on vascular geometry (tortuosity), clot characteristics  
or in cases involving atherosclerotic stenosis [6].

To date, a limited number of *in vitro* and *in silico* studies  
on the thrombectomy procedure have been reported. *In vitro*  
studies have investigated the mechanical behaviour and  
functioning of devices [17] and clots [18], and the stent–clot  
interaction [19,20]. In the few published *in silico* studies  
[21,22], the procedure was modelled as an electric circuit  
analogue and the clot as a spring-damper system, ignoring  
the mechanical nature of the stent–clot interaction.

In this regard, the increasing fascination of performing ‘virtual’  
treatment in ‘virtual’ patients [23] makes necessary the  
development of accurate *in silico* models of the thrombectomy  
procedure. An *in silico* clinical trials of AIS incorporating a  
robust *in silico* thrombectomy model would enable evaluation  
of various hypotheses on the effectiveness of thrombectomy.  
*In silico* thrombectomy models in numerous vessel geometries  
and with different clot characteristics would allow rapid  
the evaluation of the feasibility of different thrombectomy  
treatment approaches for specific patients, and patient popu-  
lations, resulting in the faster and safer introduction of new  
treatments or devices.

In this context, the objective of the current study is to  
develop an *in silico* finite element model of the thrombectomy  
procedure and to demonstrate the ability of the model to  
replicate experimental thrombectomy tests using commercial  
stents-retriever and clot analogues. To the best of our  
knowledge, this is the first finite-element model of the  
thrombectomy procedure. *In vitro* tests are also performed to  
verify the accuracy and reliability of the numerical models.  
The proposed *in vitro/in silico* comparison aims at assessing  
the applicability of the numerical model and at providing  
validation evidence for the specific *in vivo* thrombectomy  
outcomes prediction, which constitutes the ultimate *Context  
of Use* (COU). In particular, finite-element models of  
the stent-retriever and the clot are developed and their  
mechanical behaviour is calibrated with experimental tensile  
and compression tests; *in vitro* bench-top tests in different  
cerebral-like vessel geometries (idealized and anatomically  
based) are performed—and a computational simulation of  
each *in vitro* test is implemented using the *in silico* thrombectomy  
modelling framework.

## 2. Method

### 2.1. Stent-Retriever model

The EmboTrap II (CERENOVUS, Galway, Ireland) is a NiTi  
stent-retriever with a dual-layer design (figure 1a): the outer  
stent cage has large openings aimed at trapping the clot, while  
articulating leaflets maintain the contact with the arterial wall  
during retrieval, the inner channel formed by a closed-cell stent  
is aimed at trapping captured clot within the stent-retriever and  
restoring the blood flow through the clot upon deployment [24].  
The device was approved for the use in EU in late 2013 under  
the CE mark. The CAD model (5 mm outer diameter and 33 mm  
length) was analysed by means of ANSA Pre Processor v19.0  
(BETA CAE System, Switzerland) to extract the centreline of the  
frames (figure 1b). The resulting wire model was discretized  
with 4,353 Hughes-Liu beam elements with a rectangular cross  
section and average length of 0.2 mm, following a rigorous mesh  
size sensitivity analysis. In particular, three different discretiza-  
tions with an average element size of 0.4 mm, 0.2 mm and

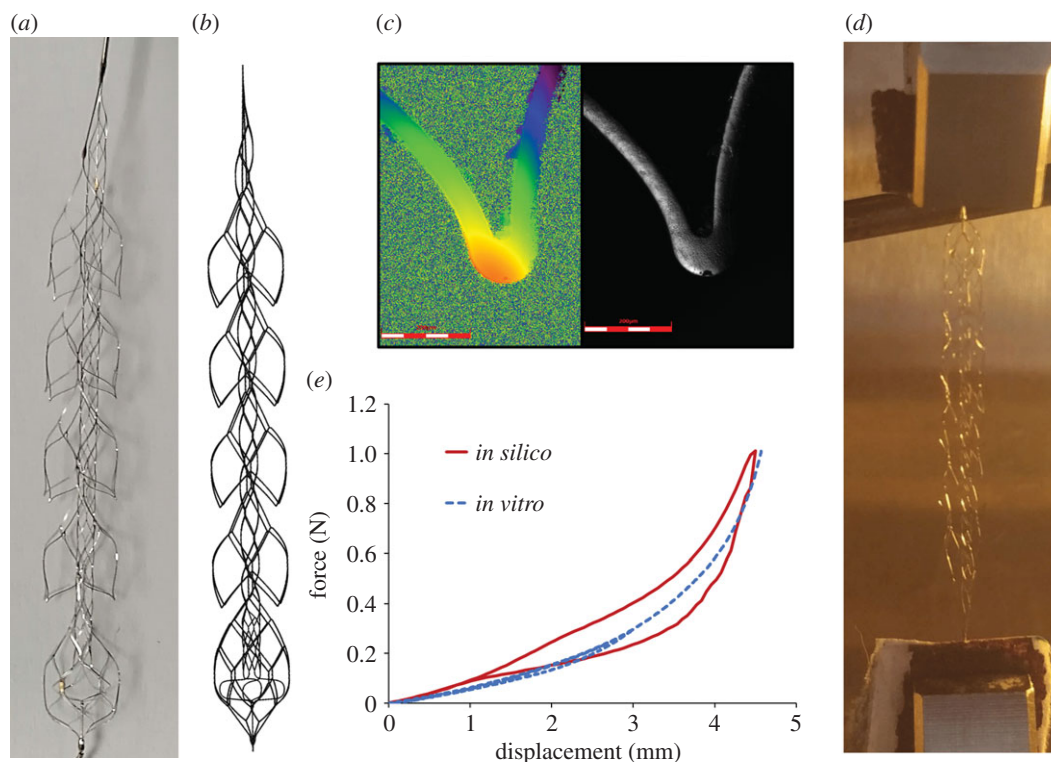


**Figure 1.** (a) EmboTrap II device and (b) its finite-element model, discretized with beam elements; (c) the stent section acquired with the confocal laser scanning microscope; (d) uniaxial tensile test and (e) the resultant force-displacement curve (dotted blue line), compared with the curve from the in silico model (solid red line).

0.1 mm were considered, with the resultant force and the axial stresses on selected elements in the central part of the device used as monitored variables for the convergence analysis. The difference in the monitored variables between the 0.2 mm and the 0.1 mm discretization was less than 3% during the crimping step of the simulations. The stent's cross sections were measured with a confocal laser scanning microscope (LEXT-OLS4100, Olympus) (figure 1c). A self-penalty hard contact between the struts of the stent was modelled in order to prevent inter-penetration of the inner parts of the retriever during the simulations.

The NiTi material parameters, provided by CERENOVUS (data not shown), were verified through a numerical-experimental coupling [25]: the stent was subjected to a uniaxial tensile test at an applied displacement rate of  $0.05 \text{ mm min}^{-1}$  until its length is extended by 4.5 mm, in a temperature-controlled chamber with air at  $37.0 \pm 0.1^\circ\text{C}$  (EnduraTEC ELF 3200, BOSE) (figure 1d). The experiment was then computationally simulated (figure 1e) and the NiTi material was modelled using the shape memory material constitutive formulation available in the commercial finite-element solver LS-DYNA 971 Release 11.0 (LSTC, Livermore, CA, USA) [26].

Crimping simulations of the device in a microcatheter with an inner diameter of 0.5 mm followed by unconstrained release were carried out to verify the crimping and release kinematic of the device. These simulations were used to determine the optimal system damping and mass scaling [27]. Internal, kinematic and dissipative energies were compared in order to guarantee quasi-static conditions during the simulation i.e. a kinetic to internal energy ratio of less than 2%. The finite-element simulations were performed on 16 CPUs of an Intel Xeon64 with 64 GB of RAM memory using the commercial finite-element solver LS-DYNA 971 Release 11.0 (LSTC, Livermore, CA, USA).

## 2.2. Clot model

Clots analogues were obtained from venous whole ovine blood using a customized protocol [28,29] (figure 2a). Unconfined compression tests of synthetic clots in 0.9% saline were performed

using a custom-built parallel plate experimental (figure 2b). Clots with a composition intermediate between red and white clots (ca. 20% RBC) were subjected to confined compression up to 80% nominal compressive strain at an applied strain rate of  $10\% \text{ s}^{-1}$ . The compressibility of the blood clot was also investigated by the processing of the images taken at different deformations during the compression test. The initial deformation of the clot at the start of the test leads to the calibration of a Poisson's ratio of 0.3.

The compression test was numerically reproduced using a simplified quasi-hyperelastic foam model defined by a single uniaxial load curve and an assumed Poisson's ratio [30]. The term quasi is used because there is really no strain energy function for determining the stresses. In this regard, the stress response mimics the gradient of the classical Hill-Ogden strain energy potential which for the case of a foam reads

$$\tau_{ii}^E = f(\lambda_i) - f(J^{-1-2\nu}),$$

where  $\tau_{ii}^E$  are the principal components of the Kirchhoff stress,  $\nu$  is the Poisson's ratio,  $\lambda_i$  the principal stretches, with  $J = \lambda_1\lambda_2\lambda_3$  the relative volume change, and  $f(\cdot)$  a function determined directly from uniaxial test data as [30]

$$f(\lambda) = \lambda g(\lambda) + \lambda^{-\nu} g(\lambda^{-\nu}) + \dots + \lambda^{(-\nu)^n} g(\lambda^{(-\nu)^n}),$$

where  $\tau = g(\lambda)$  corresponds to the experimental uniaxial curve. The formulation does not require an analytical expression for  $f(\cdot)$ ; this function consists on tabulated values of the principal stretch ratios and the input Poisson's ratio. The tabulated values are determined by LS-DYNA at the beginning of the computation in such a way that supplied data from uniaxial tension and compression tests are fitted within an arbitrarily small error, whereas linear interpolation is used to approximate the function between tabulated values. Figure 2c shows the performance of the model to replicate the unconfined compression tests.

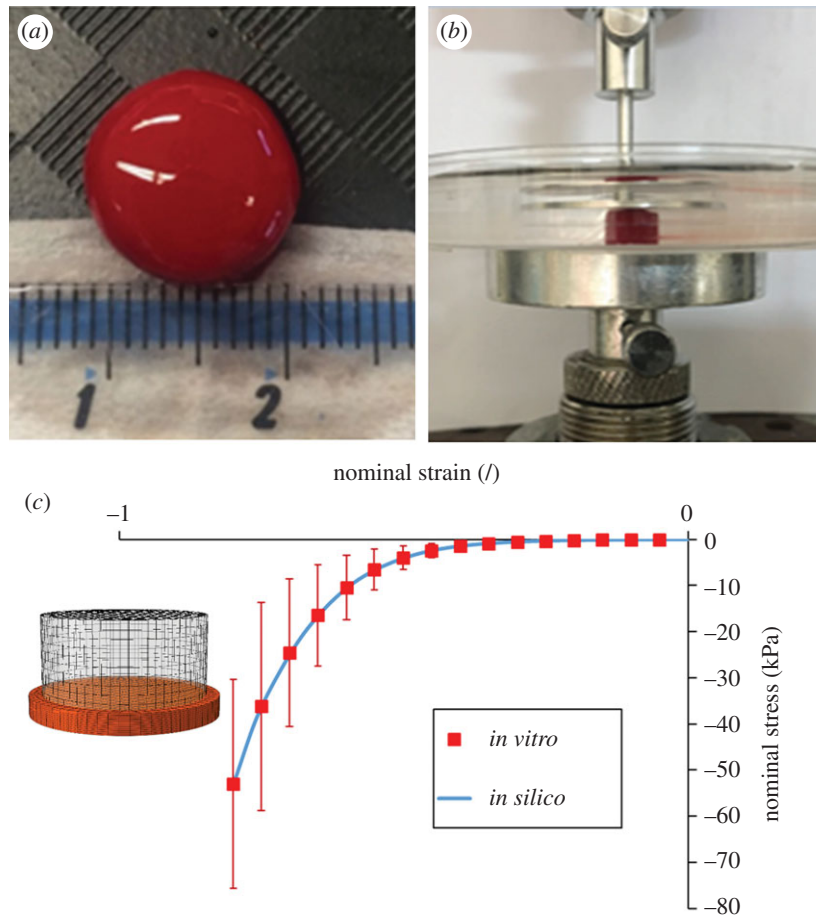


**Figure 2.** (a) Clots analogues from venous whole ovine blood; (b) unconfined compression test in saline solution; (c) the measured nominal stress–strain curve with standard deviation (dotted red line), compared with the curve from the *in silico* model (solid blue line).

### 2.3. *In vitro* thrombectomy tests

Three different functional bench tests were designed: (i) a glass U-bent vessel; (ii) a silicone funnel-shaped vessel and (iii) a patient-like three-dimensional-printed silicone vascular branch. Vessel models were fabricated with physiological dimensions in order to realistically replicate the thrombectomy procedure. Clots with the same composition (*ca.* 20%RBC) but different sizes were used. Figure 3 shows the dimensions of the different vessel models and clots considered in the study. The experiments were carried out with a stationary flow of saline solution heated at 37°C and each procedure was video recorded. Each test was performed three times in order to assure the repeatability of the outcomes.

### 2.4. *In silico* thrombectomy tests

Different clot model geometries were generated in accordance with the dimensions of the tested clot analogues. Clot model geometries were discretized with tetrahedral elements with an average size of 0.2 mm. The mesh size for the clot was chosen to be similar to that of the stent to achieve optimal simulation of the contact between the stent and the clot. A mass proportional damping of  $10 \text{ s}^{-1}$  was adopted for the clot in order to achieve stability without excessively constraining the maximum time-step [27]. The CAD models of the glass and silicone vessels were discretized with triangular rigid elements. The clots were positioned in the vessels at the same location as the *in vitro* tests. A selective mass scaling was adapted in order to have a constant time-step of  $5 \times 10^{-7} \text{ s}$ .

The finite-element models were setup in ANSA Pre Processor v19.0 (BETA CAE System, Switzerland) and the simulations were performed on 40 CPUs of an Intel Xeon64 with 256 GB of RAM memory using the commercial finite-element solver LS-DYNA.

The simulation of the thrombectomy procedure consisted of four steps:

- (i) *Stent crimping/catheter tracking*—the stent-retriever is crimped in a 0.5 mm diameter rigid straight catheter in 1 s. A hard penalty contact is defined between the stent and the catheter; at the same time, the clot is deformed and pushed against the vessel wall by the catheter. Frictionless soft penalty contact is defined between the clot and the catheter, whereas a rough soft penalty contact is defined between the clot and the vessel wall, with a friction coefficient of 0.1 in the glass vessel and of 0.2 in the silicone vessels [31].
- (ii) *Stent tracking*—the crimped stent is positioned at the location of the clot by removing it along the centreline of the guide catheter at a velocity of  $0.1 \text{ m s}^{-1}$ .
- (iii) *Deployment*—the stent is released/unsheathed by sliding the crimping catheter from the stent at a velocity of  $0.1 \text{ m s}^{-1}$ . As the stent is released it comes into contact with the clot; a soft penalty contact is defined between the stent and the clot, whereas a hard contact is implemented where the stent contacts the rigid vessel wall.
- (iv) *Retrieval*—the clot trapped by the stent following release, and the stent and trapped clot are then pulled at a velocity of  $0.05 \text{ m s}^{-1}$  along the catheter's centreline until an aspiration catheter is reached.

## 3. Results

Simulation of the crimping of the device in the catheter followed by an unconstrained release was carried out to verify the crimping and release kinematics predicted by the

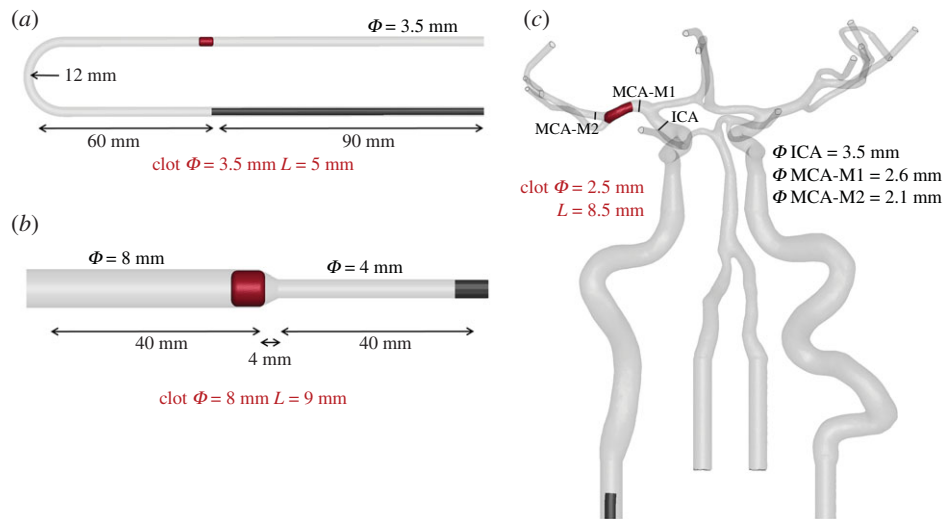


**Figure 3.** Geometry and dimensions of the three functional bench tests, (a) a glass U-bent vessel (b) a silicone funnel-shaped vessel and (c) a patient-like three-dimensional-printed silicone vascular branch. Clots' diameters and lengths are also pointed out (in red).

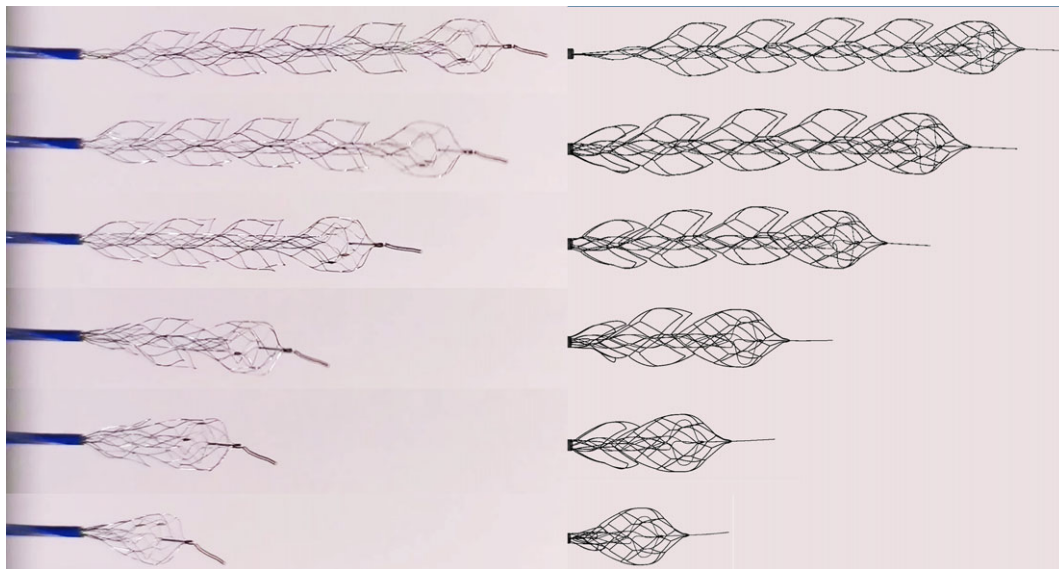


**Figure 4.** Comparison between the real (left panel) and the modelled (right panel) crimping phase of the device in the microcatheter with an inner diameter of 0.5 mm.

model. The stent model was successfully crimped in 1 s in a 0.5 mm—diameter catheter without distortion of the beam elements, element inter-penetration or instability. In figure 4, the simulation of the crimping is compared against the actual crimping of the Embo Trap II device. The unconstrained release in 1 s was also successfully modelled, the stent recovered its nominal open configuration with no residual stresses or strains. The quasi-static condition in this simulation was achieved, a mass-weighted damping factor for the stent of  $50 \text{ s}^{-1}$  and a constant time-step of  $5 \times 10^{-7} \text{ s}$  with selective element mass scaling were identified as optimum parameters.

Thrombectomy *in vitro* tests were performed and numerically reproduced. Comparison in terms of the kinematics (structure deformation) was performed, focusing in particular on the clot's position, deformation and motion. Evaluation over time of the von Mises (VM) stresses and Green von Mises (VM) strains, also known as Effective stress and strain respectively, of the clot during all the steps of the simulations was performed. Maximum stress and strain are reported as the average of the 10 elements with the maximum value,

instead of local maximum values to avoid possible spikes due to the contact of the clot with the stent or due to excessive distortion of the mesh.

The first test was conducted in a glass U-bent vessel, with a positive thrombectomy outcome. The model consisted of 48 655 finite elements and the simulation lasted 17 h. The clot, trapped into the stent's struts, was retrieved along the bend of the vessel (figure 5-left panel). In this case, the simulation successfully replicated the procedure (figure 5-right panel): during the first step (stent crimping/catheter tracking) the stent was crimped and the catheter, following the centreline of the U-bent vessel, was positioned across the clot. At this point ( $T_1$  in figure 6), the clot, pushed against the vessel wall, reached a maximum VM stress of 0.6 kPa and a VM strain of 0.25. In the stent tracking phase, the crimped stent was positioned across the clot following the centreline of the catheter, while nothing occurred on the clot, whose stress and strain values remained stable. In the deployment step, the stent was released by unsheathing the catheter. As the stent and the clot enter in contact, the stress and strain values increased in



**Figure 5.** Comparison between the *in vitro* (left panel) and the *in silico* (right panel) thrombectomy test in the glass U-bent vessel. In both the results the clot, trapped in the stent, is successfully retrieved until reaching the aspiration catheter.

the clot increase dramatically. The maximum VM stress and strain once the stent was completely released ( $T_2$  in figure 6) were 36.3 kPa and 0.72, respectively. In the third and final retrieval step, the clot is trapped between the inner and the outer layer of the stent and was retrieved following the centre-line of the catheter. During the retrieval phase, the maximum effective stress and strain in the clot decreased as the retriever pass the U-bent to further stabilize at a constant value as the retriever reaches the straight part of the vessel. In this setting, the maximum effective stress and strain in the clot resulted in 36.5 kPa and 0.78, respectively (figure 6). The second test was conducted in a silicone funnel-shaped vessel, with a negative thrombectomy outcome. The model consisted of 50 518 finite elements and the simulation lasted 18 h. In this case, the clot is not trapped within the retriever's struts during the retrieval phase and the retriever is unable to pull the clot through the

small vessel. Instead, the clot roll up in the place where the larger vessel narrows (figure 7-left panel). The simulations, again, successfully replicated the (figure 7-right panel) too. After the first stent crimping/catheter tracking step ( $T_1$  in figure 8), the clot was pushed against the vessel wall reaching a maximum VM stress of 0.4 kPa and a VM strain of 0.23, values that were maintained during the second step. During the deployment step the stent went in contact with the clot, increasing the maximum effective stress and strain values to 4.3 kPa and 0.45, respectively ( $T_2$  in figure 8). In the retrieval step, the clot, due to the significantly larger vessel to retriever diameter ratio that prevented an effective clot–stent interaction, started to roll up preventing the retriever to pull the clot into a smaller vessel. In this step, the continuous rolling of the clot produced oscillating values of the effective stressed and strains with peaks of 15.4 kPa and 0.61, respectively. The

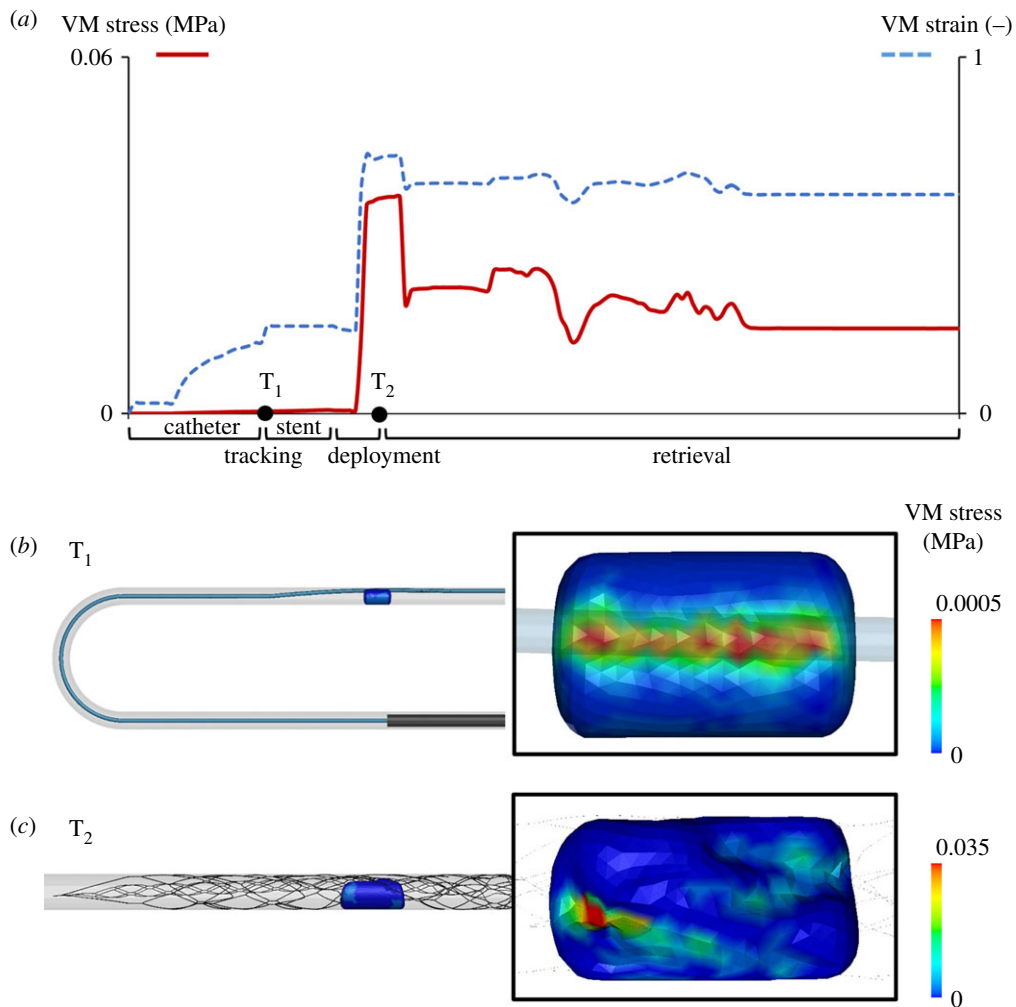


**Figure 6.** Maximum (averaged over 10 elements with the maximum values) Von Mises (VM) stress and Green von Mises (VM) strain values over time during the catheter tracking, stent tracking, deployment and retrieval steps of the simulation in the glass U-bent vessel. Von Mises stress contours on the clot in two different views at the end of the catheter tracking step (time  $T_1$ ) and at the end of the deployment step (time  $T_2$ ).

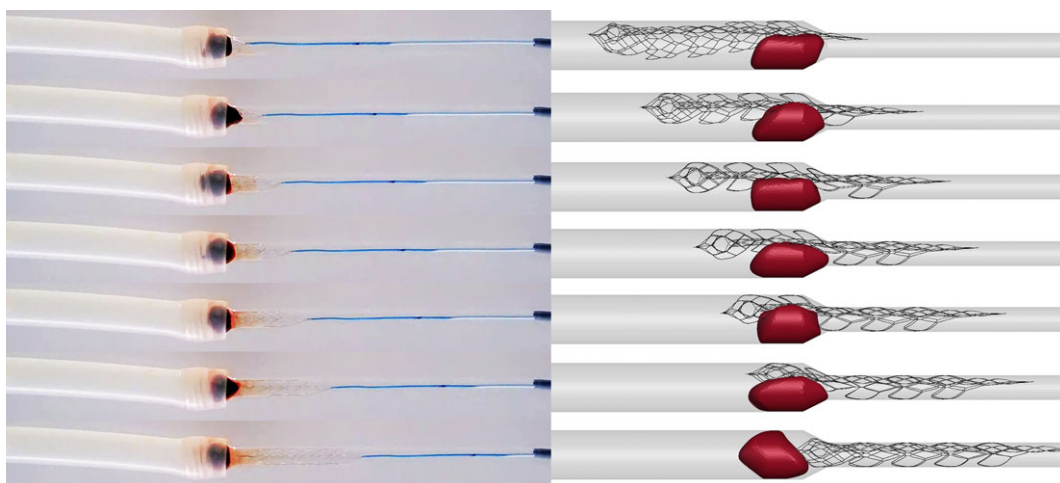


**Figure 7.** Comparison between the *in vitro* (left panel) and the *in silico* (right panel) thrombectomy test in the silicone funnel-shaped vessel. In both the results, the clot escaped from the stent by turning on itself.

third thrombectomy test was conducted in a patient-like three-dimensional-printed silicone vascular branch, with a positive outcome (figure 9-left panel). This last test is closer to the *in vivo* thrombectomy procedure. From a numerical point of view, the simulation was composed of the same four steps, but the tortuosity of the vessel increased the overall complexity

of the solution. The model consisted of 144 760 finite elements and the simulation lasted 26 h. This simulation demonstrates the robustness of the thrombectomy numerical model as it successfully replicated the experiments in terms of the successful retrieval (figure 9-right panel). In the stent crimping/catheter tracking step ( $T_1$  in figure 10), the clot was pushed against



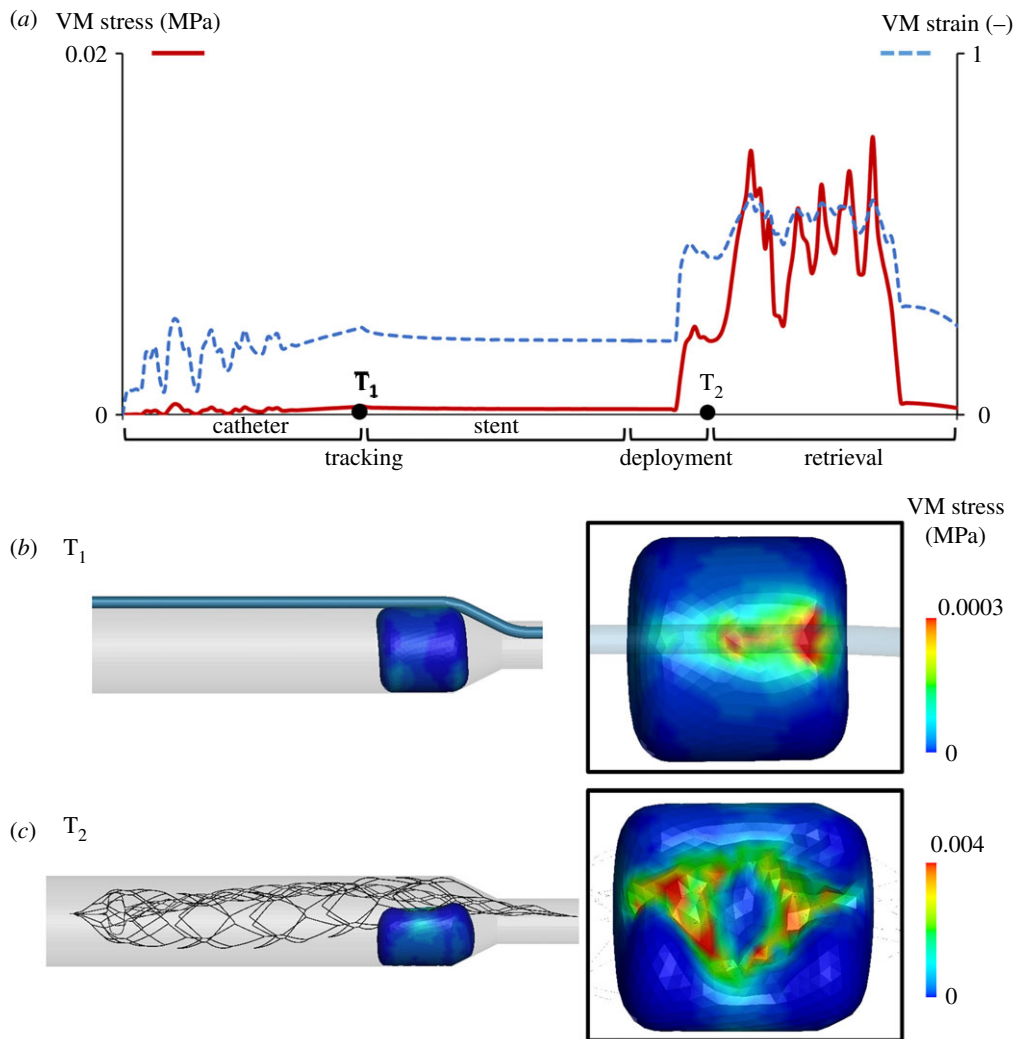


**Figure 8.** Maximum (averaged over 10 elements with the maximum values) von Mises (VM) stress and Green von Mises (VM) strain values over time during the catheter tracking, stent tracking, deployment and retrieval steps of the simulation in the silicone funnel-shaped vessel. Von Mises stress contours on the dot in two different views at the end of the catheter tracking step (time  $T_1$ ) and at the end of the deployment step (time  $T_2$ ).

the vessel wall reaching maximum effective stress of 8.0 kPa and a maximum effective strain of 0.56, values that were maintained during the second step. During the deployment step the stent went in contact with the clot, increasing the maximum effective stress and strain values to 230 kPa and 1.02, respectively ( $T_2$  in figure 10). As evidenced by these results, during the deployment phase of the retriever the clot undergoes large deformations and the stresses reach values way superior to those found in the other two experimental setups. During the retrieval phase, the clot remained trapped in the stent's struts all the way along the vessel. In this case, the open architecture of the EmboTrap II stent helped the insertion of the clot inside the stent struts [28]. During this final step, the effective stress and strain reached a maximum value of 320 kPa and 1.6, respectively.

#### 4. Discussion

In the *in silico* trial arena, numerical models of clinical procedures are becoming an important tool. Even today, numerical modelling plays a decisive role in research and the development of biomedical products. In combination with patient-specific models, *in silico* models can be used to build *in silico* clinical trials in which virtual patients are treated

with virtual treatments. On this line, in 2018, the US Food & Drug Administration (FDA) published the ASME V&V 40 technical standard 'Assessing Credibility of Computational Modeling through Verification and Validation: Application to Medical Devices' [32]. The credibility assessment begins with the statement of the Context of Use (COU) of the proposed numerical model. In this case, the COU, or in other words the specific final goal of the model, is the prediction of the thrombectomy outcomes in an ischaemic stroke patient, if the clot will be removed or not, if, consequently, the blood flow will be restored in time or not. In this view, 'would favourable validation results lead to trustworthy predictions in the Context of Use (COU)?' This is the question that the framework proposed by Pathmanathan *et al.* [33] sets out. In biomedical modelling, the issue to 'strictly' validate the numerical model is demanding due to ethical and/or technological problems. Proper validation of the thrombectomy procedure with *in vivo* measurements and images is at the moment impossible. The generation of evidence to explain the differences between the COU and the numerical model presented in this work is the cornerstone of the so-called applicability analysis.

In the thrombectomy procedure (our COU), the stent is crimped in a microcatheter with a diameter of 0.5 mm, deployed at the location of the clot in a way that, once the stent is released by unsheathing the catheter, it is in direct

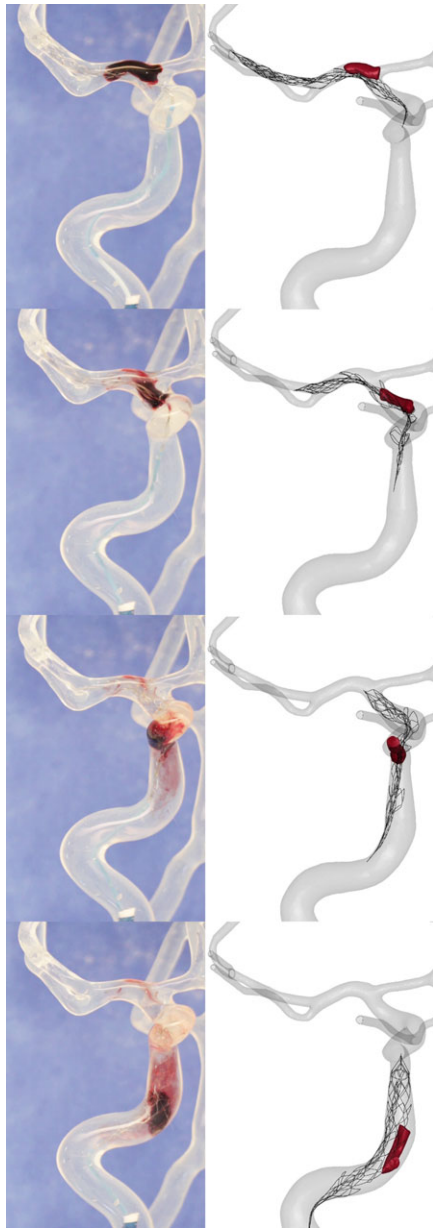


**Figure 9.** Comparison between the *in vitro* (left panel) and the *in silico* (right panel) thrombectomy test in the silicone patient-like 3D-printed vascular branch. In both the results the clot, trapped in the stent, is successfully retrieved until reaching the aspiration catheter.

contact with the clot. The clot is pushed against the arterial wall and it should be trapped by the stent struts. Finally, both the stent and the clot are removed. However, the means of the removal varies considerably. An ever-increasing list of variants to the thrombectomy procedure is being reported. In some instances, the stent-retriever is pulled to a receiving guide catheter in the extracranial ICA, in other instances, a distal access catheter is advanced to the site of the clot and stent-retriever and they are withdrawn into the catheter at that point, in other cases still, the SR is used to partially pull the clot into a distally positioned catheter and the catheter, SR and clot are removed en bloc in that configuration. In all cases, aspiration through the receiving catheter is used to aid with clot capture. In the clinical reality, different parameters could vary and affect the outcomes: the choice of the stent-retriever design and size, the patient-specific morphology of the artery branches and the clot size, location and composition.

In accordance with the clinical procedure, the finite-element analysis of the COU models the crimping, the deployment, the

release and the retrieval phases. The finite-element models of the most clinically used stents-retriever in different sizes will be available, with an equivalent section derived from the microscope observation and material model calibrated with uniaxial tensile tests. The limited availability of Ni-Ti stents prevented to perform a statistically significant experimental campaign apt at the model validation. Additional experiments, such as uniaxial, torsion and bending tests, should be performed to achieve a better degree of confidence in the model validation. Finite-element models of the clot with different sizes and compositions [1], and material behaviour calibrated with compression tests will be realized. The thrombectomy simulation will be setup with the same steps described in this work. The stent will be crimped in the 0.5 mm-diameter catheter, deployed across the clot by following the centreline of the catheter. It will be released by unsheathing the catheter, and finally, pulled along the vessel following the catheter's centreline up to the location of the aspiration catheter.

The main differences between the *in silico* thrombectomy procedure (COU) and the numerical model described in this study are the assumptions that have been adopted, which generate some limitations of the work. First, the vessel is here considered rigid instead of deformable with a nonlinear behaviour. In this study, the glass and silicon vessels of the *in vitro* model can be reasonably modelled with rigid parts, an assumption that in the COU model will be withdrawn. Second, the finite element model of the device is based on the discretization of the stent's centreline into beam elements, to which an equivalent section has been assigned. This represents a simplification which may be a source of discrepancies (in particular in terms of local strains). In addition, the dual-layer structure of the EmboTrap II stent-retriever introduces an additional difficulty to model the two parts linked together. In the current model, the two layers have been considered as a single part, contributing to stiffen the overall axial response of the *in-silico* model with respect to the actual device. Moreover, the strongly nonlinear constitutive model, such as the super-elastic material herein discussed, may lead to an intensification of the hysteresis effect in the numerical model (figure 1e), which is attributable to those elements experiencing higher strains. In the future, more efforts should be paid in a more realistic reconstruction of details of the stent geometry, in order to fully exploit the power of this computational tool for the investigation of local quantities, such as stress and strains. Third, the clot shape and material model are defined from analogues instead of from *ex vivo* clots. However, the methodology proposed by Duffy *et al.* [29] to replicate clot analogues with diverse compositions is reproducible and duplicate efficaciously *ex-vivo* clots [18]. The clot is modelled with homogeneous compressible hyperelastic material, but different aspects such as viscoelasticity, porosity and adhesion behaviour on the vessel wall could be investigated in future studies.

Moreover, if the thrombectomy procedure is preceded by thrombolysis, the size and location of the clot, drug administration time and drug dose can affect the clot mechanical properties and, consequently, the prediction of the thrombectomy simulation. Fourth, in both the thrombectomy numerical model (COU) and the numerical model described in this work, there is no blood flow. In reality, even though the procedure is usually performed with a balloon which, before the SR retraction, is inflated to arrest the antegrade flow [14], there could be some secondary flow through the collateral

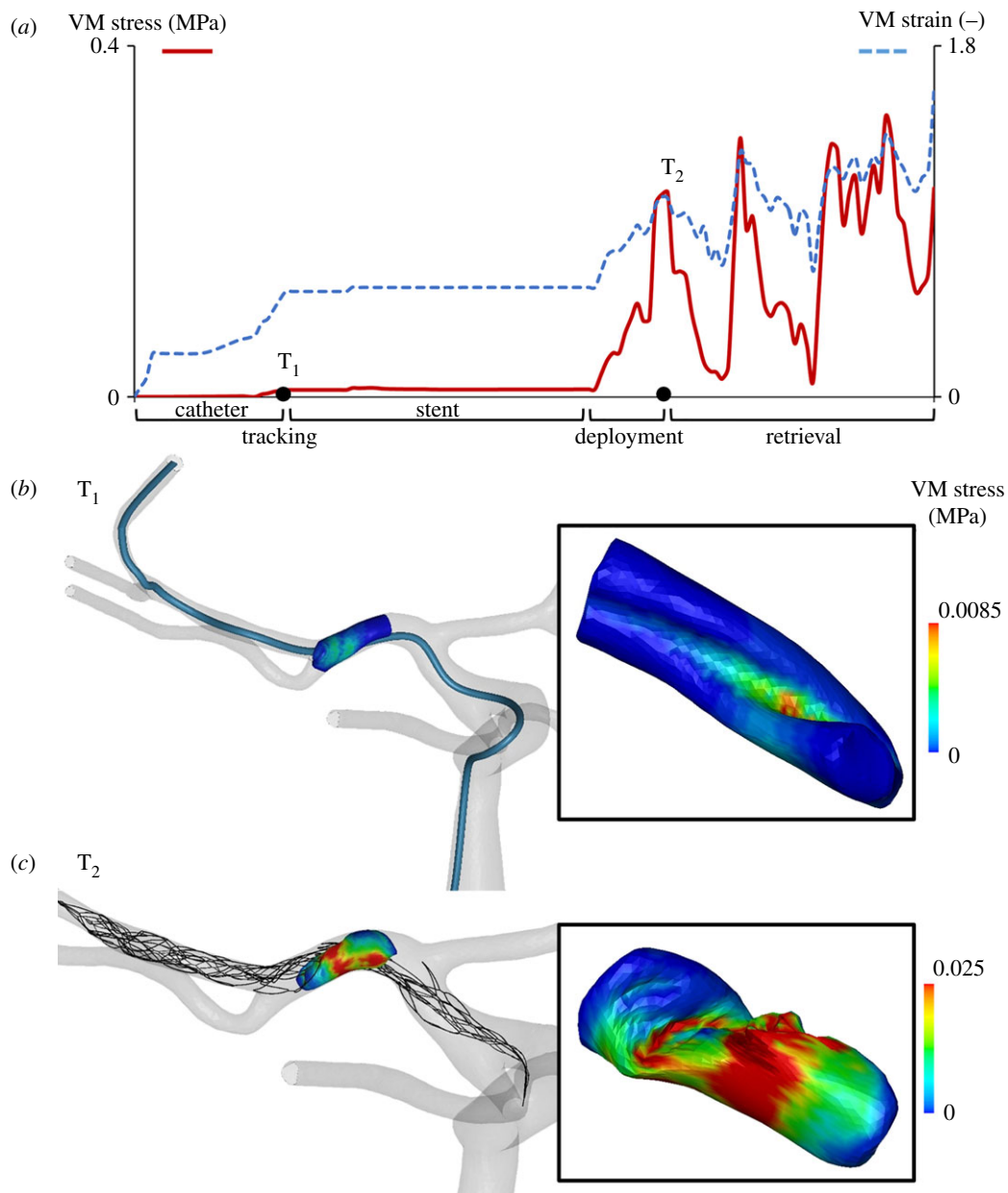


**Figure 10.** Maximum (averaged over 10 elements with the maximum values) von Mises (VM) stress and Green von Mises (VM) strain values over time during the *catheter tracking*, *stent tracking*, *deployment* and *retrieval* steps of the simulation in the silicone patient-like three-dimensional-printed vascular branch. Von Mises stress contours on the clot in two different views at the end of the *catheter tracking* step (time  $T_1$ ) and at the end of the *deployment* step (time  $T_2$ ).

circulation affecting the clot removal. Fifth, in the clinical procedure, it is common practice to wait for an embedding time during the thrombectomy to enforce the integration between clot and stent. This effect is been hypothesized to depend on the clot fibrin stretching during the stent release [28] and is not considered in both the *in silico* thrombectomy procedure (COU) and the numerical model described in this work.

The goal of a mechanical thrombectomy procedure is to completely remove a thrombus from a vessel, without loss of fragments and the goal of the relative numerical model is to predict the procedure outcome. The comparison between the *in vitro* and their equivalent in *in silico* models conducted in this study provides confidence that the numerical model is able to capture and replicate the interaction between the clot and the stent-retriever in both successful and unsuccessful procedures. Distinct validation studies were performed on the stent and the clot models, by replicating with *in silico* models the *in vitro* uniaxial tensile and unconfined compression tests. Moreover, stress and strain values from numerical models,

which are impossible to obtain from *in vivo* or *in vitro* tests, can be used once coupled with a fracture model to predict the possibility of clot fragmentation, the most important complication after thrombectomy procedure. The different stress and strain fields obtained in the different vessel geometries tests allow in future studies to consider some correlation between geometric features of the vessel—as tortuosity and diameter—and the stresses and strains on the clot.

## 5. Conclusion

The novel methodology developed shows the potential of our finite-element analysis to model all the steps of a thrombectomy procedure in an accurate way. In particular, this analysis can be used to predict potential revascularization outcomes, help to interpret adverse effects and to improve the understanding of the influence of individual patient anatomies. There is room for further improvement of the thrombectomy

631 technique, which is generally considered the most important  
632 treatment for improving the stroke treatment today. Another  
633 interesting issue is to use numerical modelling to better  
634 understand the complications of the treatment despite suc-  
635 cessful recanalization. There are still open questions about  
636 the treatments, such as the effect of the combination of throm-  
637 bolytic and stent-retriever thrombectomy and the design of  
638 new, more effective devices. Consequently, there is still  
639 room for improvement in thrombectomy device technology  
640 and the thrombectomy procedure. With the introduction of  
641 new stroke treatments, many new clinical trials are planned  
642 and expected. As such a great opportunity for thrombectomy  
643 numerical investigations exists to expedite, optimize or even  
644 replace these resource-intensive trials.

645 **Data accessibility.** This article has no additional data.

646 **Authors' contributions.** G.L. developed the finite-element thrombectomy  
647 models with the supervision of J.F.R.M. and the help of S.B.; G.D.  
648 helped supervise the research project; F.B. carried out the experimen-  
649 tal tests on the device; S.D. and A.D. carried out the thrombectomy  
650 *in vitro* tests with the supervision of R.M.C.; B.F. carried out the  
651 experimental tests on the clot analogues with the supervision of  
652 P.M.C.; C.B.L.M.M. helped supervise the project from a clinical  
653 point of view, and F.M. was in charge of overall direction and plan-  
654 ning. All authors gave final approval for publication and agree to be  
655 held accountable for the work performed therein.

656 **Competing interests.** The authors declared the following potential con-  
657 flicts of interest with respect to the research, authorship, and/or  
658 publication of this article: A.S., A.D. and R.M.C. report a financial  
659 relationship with Cerenovus outside the submitted work.

660 **Funding.** This project has received funding from the European Union's  
661 Horizon 2020 research and innovation program under grant agree-  
662 ment no. 777072.

663 **Acknowledgement.** The authors would like to thank Martina Costa  
664 Angeli for her assistance with the confocal laser scanning microscope.

## 666 Appendix: INSIST Investigators

667 Charles Majoie<sup>1</sup>, Henk Marquering<sup>1,2</sup>, Ed van Bavel<sup>2</sup>, Alfons  
668 Hoekstra<sup>3</sup>, Diederik W.J. Dippel<sup>4</sup>, Hester L. Lingsma<sup>5</sup>, Aad  
669 van der Lugt<sup>6</sup>, Noor Samuels<sup>4,5,6</sup>, Nikki Boodt<sup>4,5,6</sup>, Yvo Roos<sup>7</sup>,  
670 Simon de Meyer<sup>8</sup>, Senna Staessens<sup>8</sup>, Praneeta Konduri<sup>1,2</sup>,  
671 Nerea Arrarte<sup>2</sup>, Bastien Chopard<sup>9</sup>, Franck Raynaud<sup>9</sup>, Remy Pet-  
672 kantchin<sup>9</sup>, Vanessa Blanc-Guillemaud<sup>10</sup>, Mikhail Pantelev<sup>11,12</sup>,  
673 Alexey Shibeko<sup>11</sup>, Francesco Migliavacca<sup>13</sup>, Gabriele Dubini<sup>13</sup>,  
674 Giulia Luraghi<sup>13</sup>, Jose Felix Rodriguez Matas<sup>13</sup>, Sara Bridio<sup>13</sup>,  
675 Patrick Mc Garry<sup>14</sup>, Kevin Moerman<sup>14</sup>, Behrooz

Fereidoonzhad<sup>14</sup>, Michael Gilvarry<sup>15</sup>, Ray McCarthy<sup>15</sup>,  
Sharon Duffy<sup>15</sup>, Anushree Dwivedi<sup>15</sup>, Stephen Payne<sup>16</sup>,  
Tamas Jozsa<sup>16</sup>, Wahbi El-Bouri<sup>13</sup>, Sissy Georgakopoulou<sup>2</sup>,  
Victor Azizi<sup>3</sup>, Raymond Padmos<sup>3</sup>.

<sup>1</sup>Department of Radiology and Nuclear Medicine, Amsterdam UMC, location AMC, Amsterdam, The Netherlands;

<sup>2</sup>Biomedical Engineering and Physics, Amsterdam UMC, location AMC, Amsterdam, The Netherlands;

<sup>3</sup>Computational Science Lab, Faculty of Science, Institute for Informatics, University of Amsterdam, Amsterdam, The Netherlands;

<sup>4</sup>Department of Neurology, Erasmus MC University Medical Center, PO Box 2040, 3000 CA Rotterdam, The Netherlands;

<sup>5</sup>Department of Public Health, Erasmus MC University Medical Center, PO Box 2040, 3000 CA Rotterdam, The Netherlands;

<sup>6</sup>Department of Radiology & Nuclear Medicine, Erasmus MC University Medical Center, PO Box 2040, 3000 CA Rotterdam, The Netherlands

<sup>7</sup>Department of Neurology, Amsterdam UMC, location AMC, Amsterdam, The Netherlands;

<sup>8</sup>Laboratory for Thrombosis Research, KU Leuven Campus Kulak Kortrijk, Kortrijk, Belgium;

<sup>9</sup>Computer Science Department, University of Geneva, CUL, 7 route de Drize, 1227 Carouge, Switzerland;

<sup>10</sup>Institut de Recherches Internationales Servier, Coubevoie Cedex, France;

<sup>11</sup>Center for Theoretical Problems of Physicochemical Pharmacology RAS, Moscow, Russia;

<sup>12</sup>Dmitry Rogachev National Research Center of Pediatric Hematology, Oncology and Immunology, Moscow, Russia; Faculty of Physics, Lomonosov Moscow State University, Moscow, Russia;

<sup>13</sup>Department of Bioengineering and Laboratory of Biological Structure Mechanics-LaBS, Politecnico di Milano, Piazza Leonardo da Vinci 32, 20133 Milano, Italy.

<sup>14</sup>College of Engineering and Informatics, National University of Ireland Galway, Ireland; National Centre for Biomedical Engineering Science, National University of Ireland Galway, Ireland;

<sup>15</sup>Cerenovus, Galway Neuro Technology Centre, Galway, Ireland;

<sup>16</sup>Institute of Biomedical Engineering, Department of Engineering Science, University of Oxford, Parks Road, Oxford OX1 3PJ, UK.

## 680 References

- 681 1. Gersh KC, Nagaswami C, Weisel JW. 2009 Fibrin network structure and clot mechanical properties are altered by incorporation of erythrocytes. *Thromb. Haemost.* **102**, 1169–1175. (doi:10.1160/TH09-03-0199)
- 682 2. Wintermark M *et al.* 2013 Imaging Recommendations for acute stroke and transient ischemic attack patients: a joint statement by the American Society of Neuroradiology, the American College of Radiology, and the Society of NeuroInterventional Surgery. *Am. J. Neuroradiol.* **34**, E117–E127. (doi:10.3174/ajnr.A3690)
- 683 3. Saver JL. 2006 Time is brain—quantified. *Stroke* **37**, 263–266. (doi:10.1161/01.STR.0000196957.55928.ab)
- 684 4. Raychev R, Saver JL. 2012 Mechanical thrombectomy devices for treatment of stroke. *Neurol. Clin. Pract.* **2**, 231–235. (doi:10.1212/CPJ.0b013e31826af206)
- 685 5. Nogueira RG *et al.* 2018 Safety and efficacy of a 3-dimensional stent retriever with aspiration-based thrombectomy vs aspiration-based thrombectomy alone in acute ischemic stroke intervention. *JAMA Neurol.* **75**, 304. (doi:10.1001/jamaneurol.2017.3967)
- 686 6. Kang D-H, Park J. 2017 Endovascular stroke therapy focused on stent retriever thrombectomy and direct clot aspiration: historical review and modern application. *J. Korean Neurosurg. Soc.* **60**, 335. (doi:10.3340/JKNS.2016.0809.005)
- 687 7. Fanous AA, Siddiqui AH. 2016 Mechanical thrombectomy: Stent retrievers vs. aspiration

- 694 catheters. *Cor Vasa* **58**, e193–e203. (doi:10.1016/j.  
695 crvasa.2016.01.004)
- 696 8. Mattle HP *et al.* 2019 Analysis of revascularisation in  
697 ischaemic stroke with EmboTrap (ARISE I study) and  
698 meta-analysis of thrombectomy. *Interv. Neuroradiol.*  
699 **25**, 261–270. (doi:10.1177/1591019918817406)
- 700 9. Samaniego EA, Dabus G, Linfante I. 2011 Stenting  
701 in the treatment of acute ischemic stroke: literature  
702 review. *Front. Neurol.* **2**, 76. (doi:10.3389/fneur.  
703 2011.00076)
- 704 10. Campbell BCV *et al.* 2015 Endovascular therapy for  
705 ischemic stroke with perfusion-imaging selection.  
706 *N. Engl. J. Med.* **372**, 1009–1018. (doi:10.1056/  
707 NEJMoa1414792)
- 708 11. Zaidat OO *et al.* 2018 Primary results of the  
709 multicenter ARISE II Study (analysis of  
710 revascularization in ischemic stroke with embotrap).  
711 *Stroke* **49**, 1107–1115. (doi:10.1161/STROKEAHA.  
712 117.020125)
- 713 12. Nogueira RG *et al.* 2012 Trevo versus Merci retrievers  
714 for thrombectomy revascularisation of large vessel  
715 occlusions in acute ischaemic stroke (TREVO 2):  
716 a randomised trial. *Lancet* **380**, 1231–1240.  
717 (doi:10.1016/S0140-6736(12)61299-9)
- 718 13. Berkhemer OA *et al.* 2015 A randomized trial of  
719 intraarterial treatment for acute ischemic stroke.  
720 *N. Engl. J. Med.* **372**, 11–20. (doi:10.1056/  
721 NEJMoa1411587)
- 722 14. Chueh J-Y, Kühn AL, Puri AS, Wilson SD, Wakhloo  
723 AK, Gounis MJ. 2013 Reduction in distal emboli  
724 with proximal flow control during mechanical  
725 thrombectomy. *Stroke* **44**, 1396–1401. (doi:10.  
726 1161/STROKEAHA.111.670463)
- 727 15. Berger C, Fiorelli M, Steiner T, Schübitz WR, Bozzao  
728 L, Bluhmki E, Hacke W, von Kummer R. 2001  
729 Hemorrhagic transformation of ischemic brain  
730 tissue: asymptomatic or symptomatic? *Stroke* **32**,  
731 1330–1335. (doi:10.1161/01.STR.32.6.1330)
- 732 16. Leishangthem L, Satti SR. 2014 Vessel perforation  
733 during withdrawal of Trevo ProVue stent retriever  
734 during mechanical thrombectomy for acute ischemic  
735 stroke. *J. Neurosurg.* **121**, 995–998. (doi:10.3171/  
736 2014.4.JNS132187)
- 737 17. Machi P, Jourdan F, Ambard D, Reynaud C, Lobotesis  
738 K, Sanchez M, Bonafé A, Costalat V. 2017  
739 Experimental evaluation of stent retrievers'  
740 mechanical properties and effectiveness.  
741 *J. Neurointerv. Surg.* **9**, 257–263. (doi:10.1136/  
742 neurintsurg-2015-012213)
- 743 18. Johnson S, Duffy S, Gunning G, Gilvarry M, McGarry  
744 JP, McHugh PE. 2017 Review of mechanical testing  
745 and modelling of thrombus material for vascular  
746 implant and device design. *Ann. Biomed. Eng.* **45**,  
747 2494–2508. (doi:10.1007/s10439-017-1906-5)
- 748 19. Ohshima T, Kawaguchi R, Nagano Y, Miyachi S,  
749 Matsuo N, Takayasu M. 2019 Experimental direct  
750 measurement of clot-capturing ability of stent  
751 retrievers. *World Neurosurg.* **121**, e358–e363.  
752 (doi:10.1016/j.wneu.2018.09.106)
- 753 20. van der Marel K *et al.* 2016 Quantitative assessment  
754 of device-clot interaction for stent retriever  
755 thrombectomy. *J. Neurointerv. Surg.* **8**, 1278–1282.  
756 (doi:10.1136/neurintsurg-2015-012209)
- 757 21. Romero G, Martinez L, Maroto J, Pearce G. 2012  
758 A comparison of the removal of blood clots by  
759 mechanical thrombectomy devices using auto-  
760 expandable stents and suction pressure devices |  
761 Request PDF. *Int. J. Simul. Syst. Sci. Technol.* **13**,  
762 81–88.
- 763 22. Talayero C, Romero G, Pearce G, Wong J. 2019  
764 Numerical modelling of blood clot extraction by  
765 aspiration thrombectomy. Evaluation of aspiration  
766 catheter geometry. *J. Biomech.* **94**, 193–201.  
767 (doi:10.1016/j.jbiomech.2019.07.033)
- 768 23. Pappalardo F, Russo G, Tshinanu FM, Viceconti M.  
769 2018 In silico clinical trials: concepts and early  
770 adoptions. *Brief. Bioinform.* bby043. (doi:10.1093/  
771 bib/bby043)
- 772 24. Kabbasch C *et al.* 2016 First-in-man procedural  
773 experience with the novel embotrap®  
774 revascularization device for the treatment of  
775 ischemic stroke—a European multicenter series.  
776 *Clin Neuroradiol* **26**, 221–228. (doi:10.1007/s00062-  
777 014-0352-0)
- 778 25. Allegretti D, Berti F, Migliavacca F, Pennati G, Petrini  
779 L. 2018 Fatigue assessment of nickel–titanium  
780 peripheral stents: comparison of multi-axial fatigue  
781 models. *Shape Mem. Superelasticity* **4**, 186–196.  
782 (doi:10.1007/s40830-018-0150-7)
- 783 26. Livermore Software Technology Corporation (LSTC).  
784 2018 *LS-DYNA Theory Manual*.
- 785 27. Luraghi G, Migliavacca F, Rodriguez Matas JF. 2018  
786 Study on the accuracy of structural and FSI heart  
787 valves simulations. *Cardiovasc. Eng. Technol.* **9**,  
788 1–16. (doi:10.1007/s13239-018-00373-3)
- 789 28. Weafer FM, Duffy S, Machado I, Gunning G,  
790 Mordasini P, Roche E, McHugh PE, Gilvarry M. 2019  
791 Characterization of strut indentation during  
792 mechanical thrombectomy in acute ischemic stroke  
793 clot analogs. *J. Neurointerv. Surg.* **11**, 891–897.  
794 (doi:10.1136/neurintsurg-2018-014601)
- 795 29. Duffy S *et al.* 2017 Novel methodology to replicate  
796 clot analogs with diverse composition in acute  
797 ischemic stroke. *J. Neurointerv. Surg.* **9**, 486–491.  
798 (doi:10.1136/neurintsurg-2016-012308)
- 799 30. Kolling S, Du Bois PA, Benson DJ, Feng WW. 2007  
800 A tabulated formulation of hyperelasticity with rate  
801 effects and damage. *Comput. Mech.* **40**, 885–899.  
802 (doi:10.1007/s00466-006-0150-x)
- 803 31. Gunning GM, McArdle K, Mirza M, Duffy S, Gilvarry  
804 M, Brouwer PA. 2018 Clot friction variation with  
805 fibrin content; implications for resistance to  
806 thrombectomy. *J. Neurointerv. Surg.* **10**, 34–38.  
807 (doi:10.1136/neurintsurg-2016-012721)
- 808 32. In press. See <https://www.asme.org/codes-standards/find-codes-standards/v-v-40-assessing-credibility-computational-modeling-verification-validation-application-medical-devices>.
- 809 33. Pathmanathan P, Gray RA, Romero VJ, Morrison TM.  
810 2017 Applicability analysis of validation evidence for  
811 biomedical computational models. *J. Verif. Valid.*  
812 *Uncertain. Quantif.* **2**, 021005. (doi:10.1115/1.  
813 4037671)